*Supporting Information for:*

# Knocking down the kinetic barriers towards fast-charging and low-temperature sodium metal batteries

Xueying Zheng,[1] Zhenyi Gu,[2] Jing Fu,[1,*] Haotian Wang,[1] Xiaolu Ye,[1] Liqiang Huang,[1] Xuyang Liu,[1] Xinglong Wu,[2] Wei Luo,[1,*] Yunhui Huang[1,*]

[1]Institute of New Energy for Vehicles, Shanghai Key Laboratory of Development & Application for Metallic Functional Materials, School of Materials Science and Engineering, Tongji University, Shanghai 201804, China

E-mail: weiluo@tongji.edu.cn; jingfu@tongji.edu.cn; huangyh@tongji.edu.cn

[2]Key Laboratory for UV Light-Emitting Materials and Technology of Ministry of Education, National and Local United Engineering Laboratory for Power Batteries, Faculty of Chemistry, Northeast Normal University, Changchun, Jilin 130024, China

* Corresponding authors

## EXPERIMENTAL PROCEDURES

### Electrolyte Preparation

The battery-grade $NaPF_6$, FEC, EMC and HFE and the as-prepared 1 M $NaPF_6$ in EC/PC electrolyte were purchased from Duoduo chemical reagent Co., LTD. Prior to electrolyte preparation, the salt was vacuum-dried at 100ºC overnight in a chamber attached to the glovebox, and solvents were dried using the treated molecular sieves. All the processes were carried out inside the MIKROUNA glovebox with both $H_2O$ and $O_2$ content less than 0.1 ppm.

### Fabrication of the $Na_3V_2(PO_4)_2O_2F$ (NVPOF) Cathode

The NVPOF powder was synthesized using hydrothermal method as previously reported in our work.[1] Specifically, $H_2C_2O_4$ and $V_2O_5$ were dissolved in distilled water with molar ratio of 3:1, followed by constant stirring for 1 h at 70°C. Then, stoichiometric amount of $NH_4H_2PO_4$ and NaF were added into the solution with continuous stirring applied. The pH of the solution was subsequently adjusted by ammonium hydroxide to 7.0 ± 0.05, with the as-obtained solution transferred into Teflon-lined autoclave and heated for 12 h at 170°C. The NVPOF materials were vacuum-dried after being centrifugated with ethanol for 3 times. The NVPOF cathodes were prepared by mixing NVPOF, super-P and CMC at 7:2:1 by weight, and then vacuum-dried at 100°C for 12 h after being casted on a Al current collector.

### Fabrication of the bare Na and Na-SF anode

Na metal strips were firstly obtained through a cutting and pressing process from the as-obtained Na cubes (Sigma Aldrich, 99.9%). Bare Na anode was acquired by punching Na strips into disks with needed diameter (Φ=12 mm for coin-cells and Φ=40 mm for cell models). The Na-SF anode was realized though plastering the $SnF_2$ powders (Sigma Aldrich, 99%) on Na metal, followed by pressing with roller squeezer, by which a spontaneous reaction was triggered between Na metal and $SnF_2$ to produce $Na_{15}Sn_4$ alloy with NaF on their

contacted interface. The procedures were all performed in the Ar-filled glovebox ($H_2O$ and $O_2$ content < 0.1 ppm).

**Characterizations**

Raman spectra of the electrolytes were recorded with the LabRAM HR Evolution instrument (632.8 nm excitation laser). The electrolyte conductivity and viscosity were tested on the conductivity measuring meter (DDS-307, Leici, China) and the Thermo HAAKE MARS 60 with a rotator of 60 mm in diameter at corresponding temperatures, respectively. Analysis on electrolyte wettability was determined by recording contact angles on the separators via Dataphysics OCA50AF. Electrolyte flammability were determined using glass-fiber separators immersed with the corresponding electrolyte, followed by ignition with a flaming torch. SEM analysis was performed on Zeiss Sigma 300VP equipped with Aztec X-Max 80 for EDX mappings. HRTEM and HAADF-STEM characterizations were carried out using Tecnai G2 F20 S-Twin. XRD characterizations were conducted on PANalytical X'Pert PRO MRD diffractometer with Ni-filtered Cu Kα radiation, during which the metallic Na samples were sealed with Kapton tape to avoid contact with the air. XPS measurements (American Thermo Fisher Scientific ESCALAB 250Xi) were used to characterize the compositions of the SEI and CEI formed in the respective electrolyte, with argon-filled transfer vessel applied to load the samples during transfer. Prior to characterizations, all the retrieved electrodes were rinsed with EMC solvent for 3 times and dried thoroughly in the vacuum-chamber attached to the glovebox.

**Calculation Methods**

MD simulations were carried out using Gromacs program suite with all-atom optimized potentials for the liquid simulations (OPLS-AA) force field.[2] The force field parameters (OPLS-2009IL) of the $PF_6^-$ anion were acquired from the literatures, and a charge scaling of

0.8 was used to mimic polarization and the charge transfer effects.[3, 4] Force field parameters of the EC, PC, FEC, EMC and HFE molecules were obtained from the LigParGen web server.[5] The simulation box was set at a dimension of 50×50×50 $Å^3$ packed with the corresponding electrolyte salt/solvents using the Packmol program.[6] The structures were priorly relaxed with the energy minimizing calculations, followed by annealing at 0-298.15 K with a time step of 1ps until reach the equilibrium, the whole process was lasted for 1 ns. To maintain a temperature at 298.15 K, velocity-rescale thermostat was adopted with a relaxation constant of 1 ps.[7] Berendsen's barostat was applied to control the pressure at $1.01325\times10^5$ Pa with a isothermal compressibility constant of $4.5\times10^{-5}$.[8] The electrostatic interactions and van der Waals forces were treated with the Particle-mesh Ewald (PME) method at a cut-off distance of 10 Å.[9] The MD simulation was run for a total time of 10 ns, with the trajectory saved for each 1 ps. The further statistics were analyzed from the simulated trajectory data using the Gromacs tool-suites, the Visual Molecular Dynamic (VMD) program and some python scripts written by ourselves.[10]

The $Na^+$-solvent pairs were optimized under framework of the density of functional theory (DFT) with PBE0 functional and def2SVP basis set.[11, 12] The binding energy between $Na^+$ ions and the solvent molecules was calculated from the formular:

$$E_{binding} = E_{complex} - E_{solvent} - E_{Na+}$$

where $E_{\text{complex}}$ stands for the total energy of the complex with solvent molecules binded with $Na^+$ ions; $E_{\text{Na+}}$ and $E_{\text{solvent}}$ refer to the energy of the individual $Na^+$ ion and the solvent molecules, respectively.

**Electrochemical Measurements**

For coin cell configurations, 2032-type coin cells are fabricated using glass fiber separator (Whatman GF/D) with 180 μL electrolyte per cell. The home-made cell models were employed by further assessing practicality of the full cells, where the Na anode and NVPOF

cathode were prepared at diameters of 42 mm. The cycling and rate behavior of the cells were tested on a standard battery tester (Neware, CT4008). EIS, CV and LSV measurements were carried out using Biologic VMP-3 multi-channel workstation. Detailedly, EIS was obtained at a frequency range of 10 mHZ to $10^3$ kHZ, whereas the CV curves were recorded in Na/Na symmetric cell from -0.15 to 0.15 V.

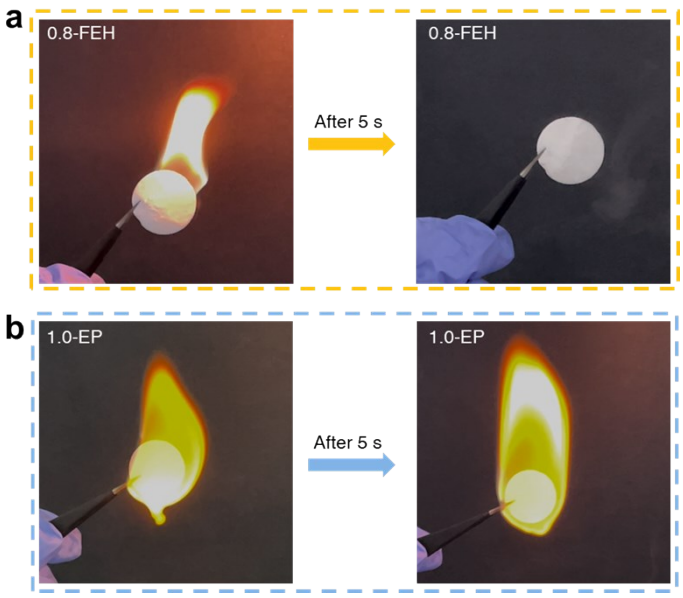


**Figure S1.** Flammability tests of the (a) 1.0-EP and the (b) 0.8-FEH electrolyte with the corresponding electrolyte soaked in glass-fiber separator. Notably, though the 0.8-FEH electrolyte is ignitable at the beginning, it self-distinguishes after 5 s, which is benefitted from the high fluorination degree of HFE that effectively captures the oxygen and hydrogen radicals to quench the fire.[13, 14] By contrast, the conventional carbonate electrolyte of 1.0-EP keeps igniting througout the process, posing sereve safety issues especially when pairing with the highly-reactive Na metal anode.

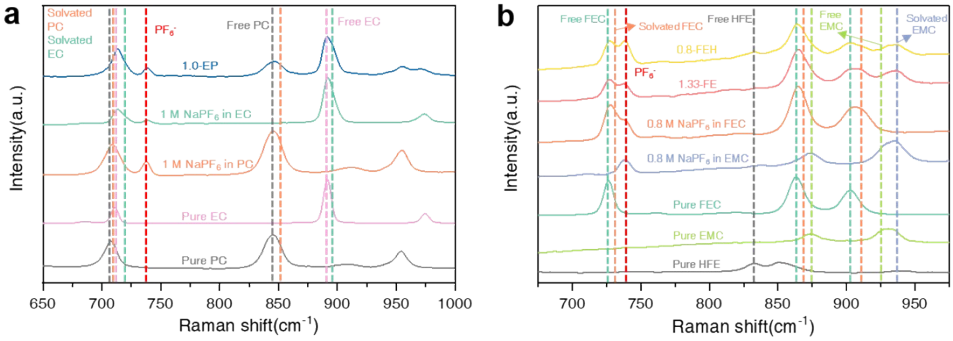


**Figure S2.** Raman spectra of the corresponding electrolyte systems. Raman peaks related to the species within the (a) 1.0-EP electrolyte and the (b) 1.33-FE and 0.8-FEH electrolytes. Here, to identify the sources of each peak in the corresponding electrolyte, we prepared the rest solutions and related the peaks accordingly. The Raman spectrum of the 1.0-EP electrolyte can be deconvoluted into peaks of free EC, free PC and solvated EC, solvated PC molecules and the $PF_6^-$ anions. The 1.33-FE electrolyte shows peaks corresponding to free FEC, free EMC and solvated FEC, solvated EMC molecules and the $PF_6^-$ anions. The introduction of HFE brings new peaks assigned to HFE solvent for the 0.8-FEH electrolyte.

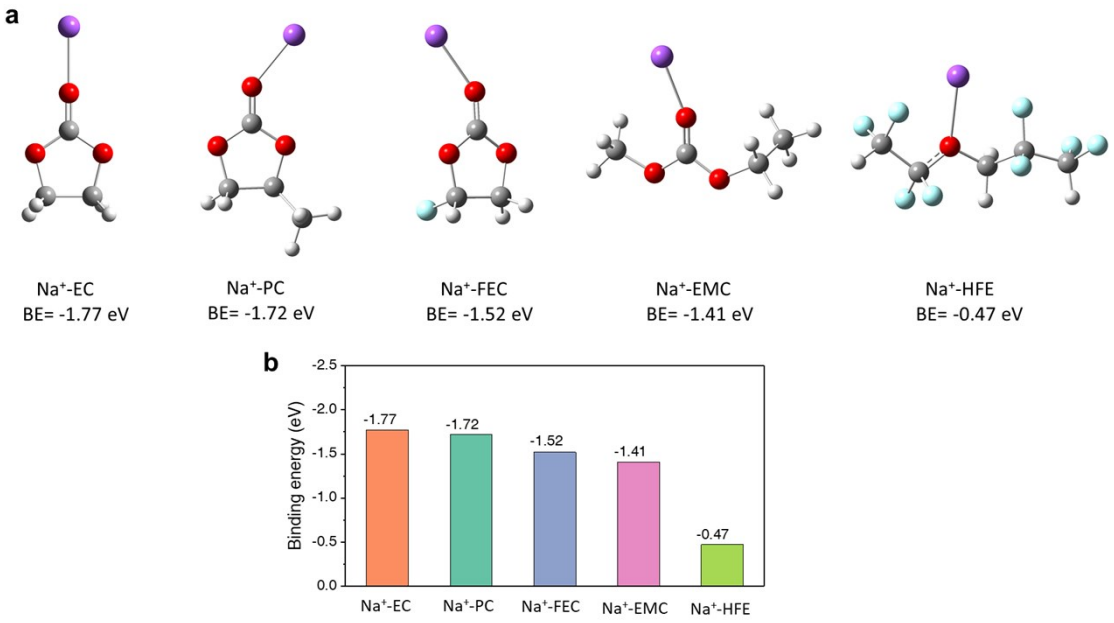


**Figure S3.** (a) The optimized geometrical configuration of the corresponding $Na^+$/solvent pairs with the binding energy (BE) marked below. The Na, C, O, H and F were marked with purple, grey, red, white and cyan, respectively. (b) Bar chart comparing the binding energies of the corresponding $Na^+$/solvent pairs.

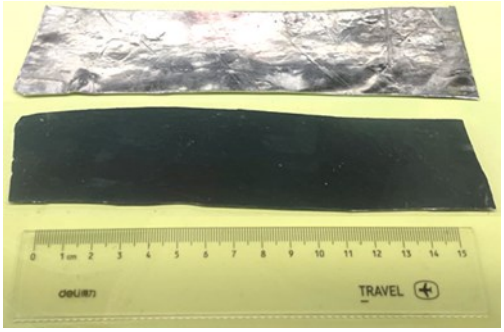


**Figure S4.** Optical image of the bare Na metal foil (silver color) and the as-prepared Na-SF anode (black color). The color change (from silver to black) was instant after applying $SnF_2$ powders on bare Na followed by a roller-pressing process, suggestive of the spontaneous reaction between $SnF_2$ and the metallic Na.

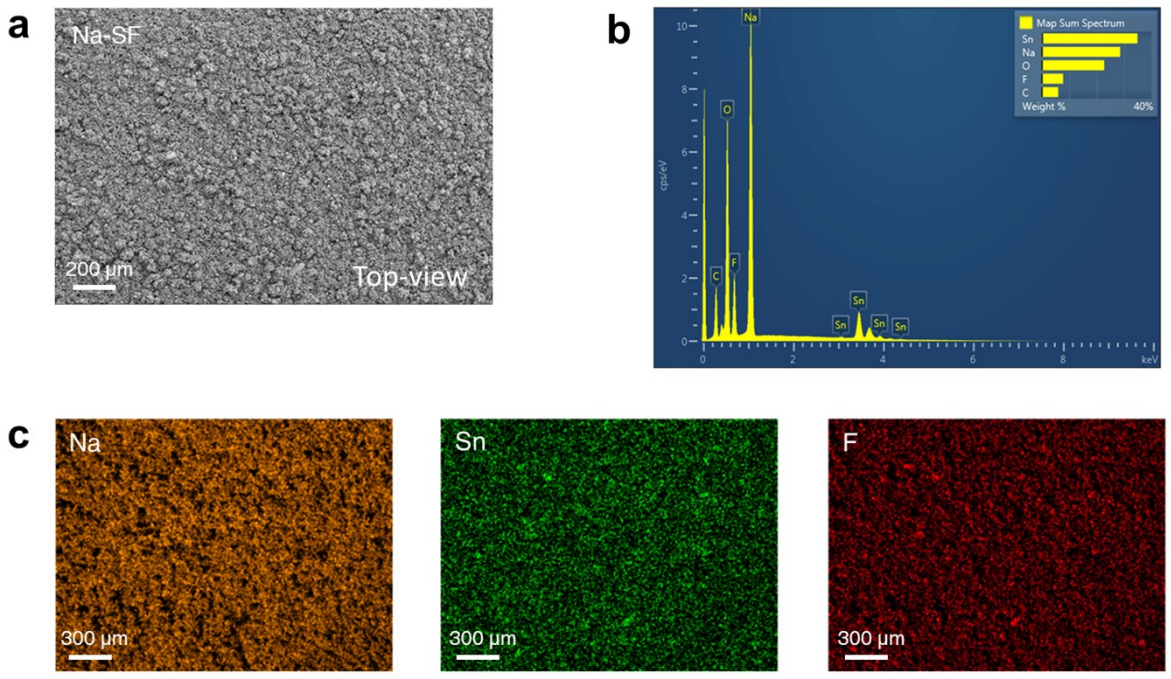


**Figure S5.** (a) Top-view SEM image of the Na-SF anode with the corresponding (b) EDX full spectra and mapping of the (c) Na, Sn and F elemental signals. Surface of the Na-SF electrode shows a compact and particle-agglomerated morphology, with Na, Sn and F signals uniformly distributing on the electrode, indicating a complete and homegeneous reaction taken place.

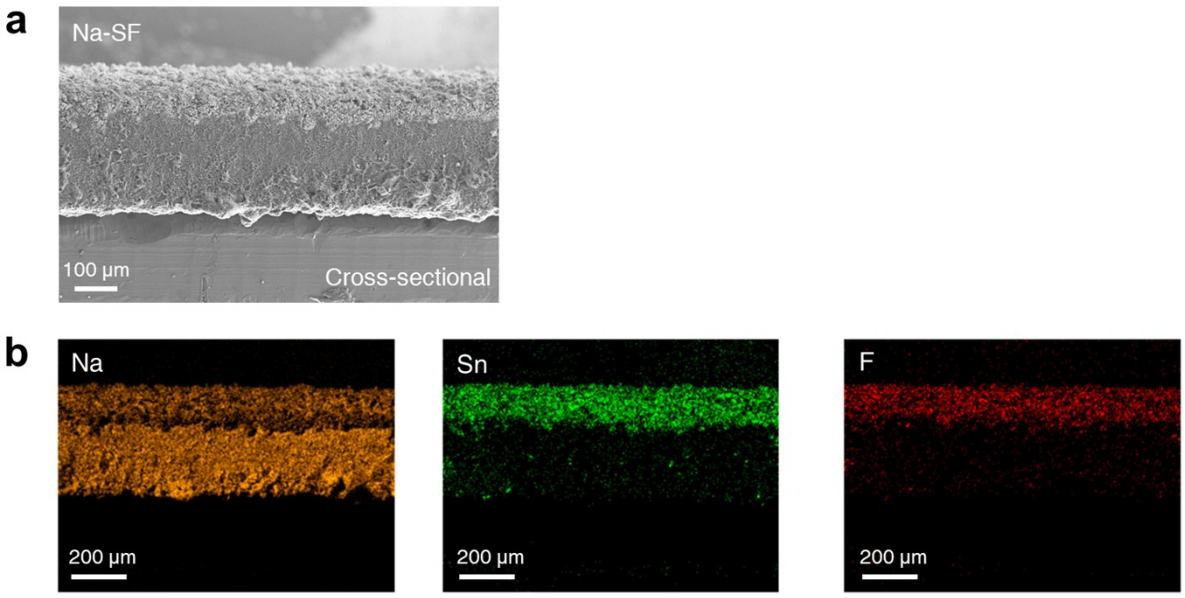


**Figure S6.** (a) Cross-sectional SEM image of the Na-SF anode with the corresponding (b) mapping of the (c) Na, Sn and F elemental signals. An additional layer is clearly seen to uniformly cover on Na metal, with conformal distribution of the Na, Sn, and F signals within the formed layer.

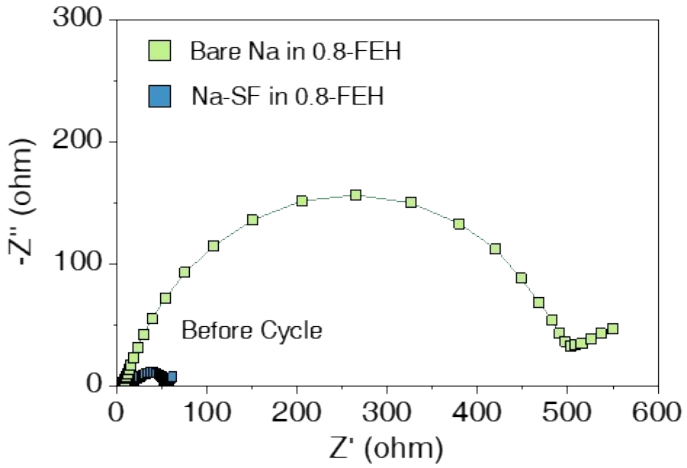


**Figure S7.** Nyquist plots of the symmetric cells with bare Na and Na-SF electrodes in the 0.8-FEH electrolyte before cycling.

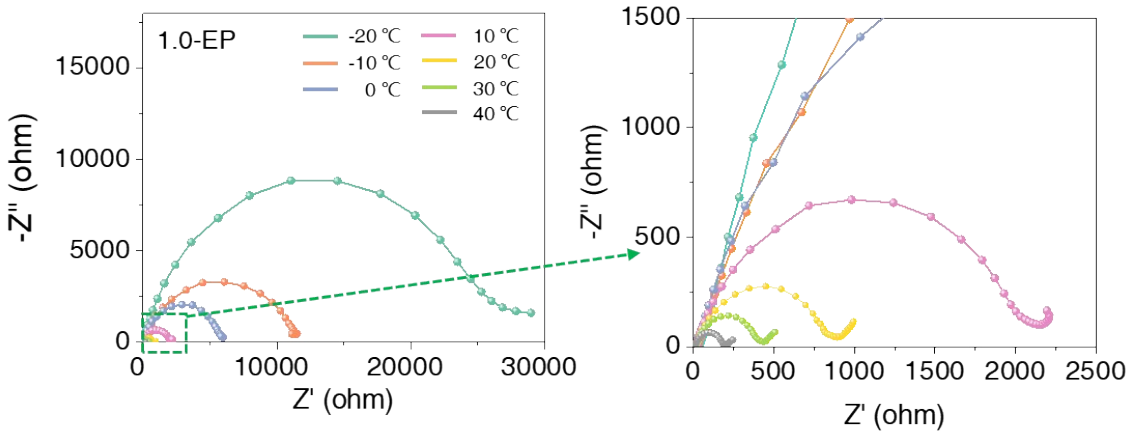


**Figure S8.** Nyquist plots of the Na/Na symmetric cells using the 1.0-EP electrolyte at temperatures from -20 to 40℃ after 3 formation cycles at 1 mA/cm$^2$ with a capacity of 1 mAh/cm$^2$.

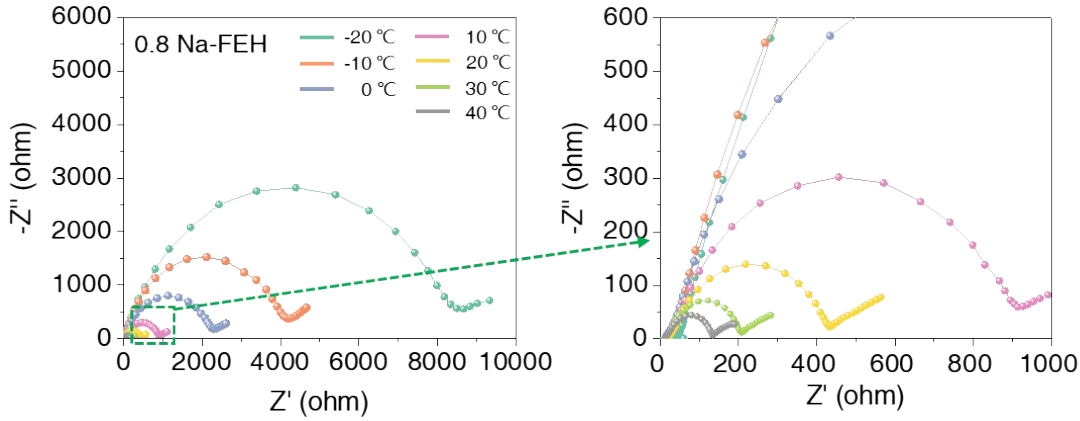


**Figure S9.** Nyquist plots of the Na/Na symmetric cells using the 0.8-FEH electrolyte at temperatures from -20 to 40℃ after 3 formation cycles at 1 mA/cm$^2$ with a capacity of 1 mAh/cm$^2$.

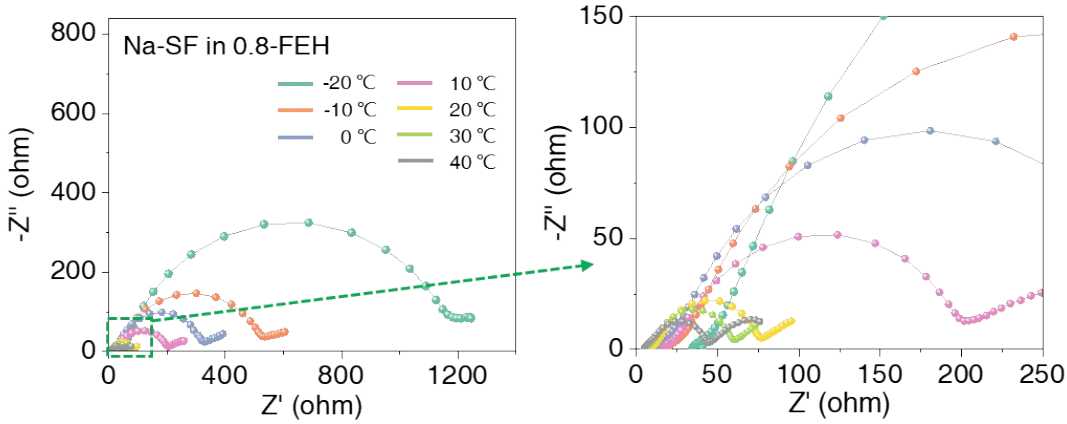


**Figure S10.** Nyquist plots of the Na-SF/Na-SF symmetric cells using the 0.8-FEH electrolyte at temperatures from -20 to 40℃ after 3 formation cycles at 1 mA/cm$^2$ with a capacity of 1 mAh/cm$^2$.

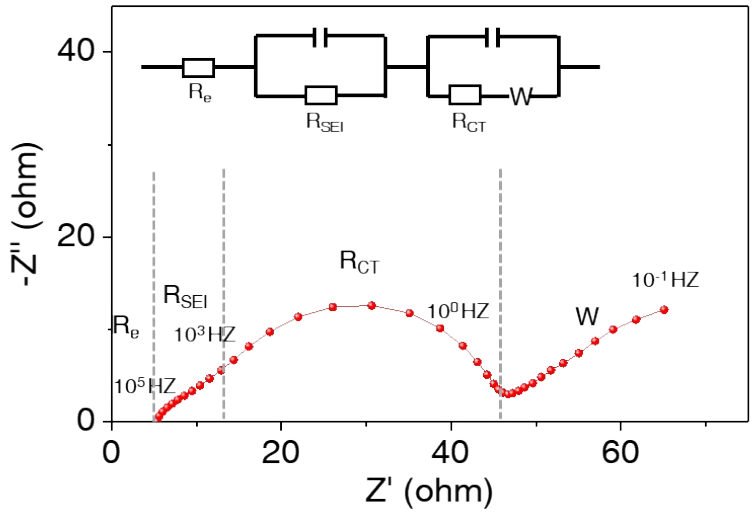


**Figure S11.** The equivalent circuit model used to fit the Nyquist plots of the symmetric cells. $R_e$, $R_{SEI}$ (high-middle frequency region) and $R_{CT}$ (low frequency region) stands for the impedance of the bulk electrolyte, the $Na^+$ diffusion through SEI and de-solvation process, respectively.

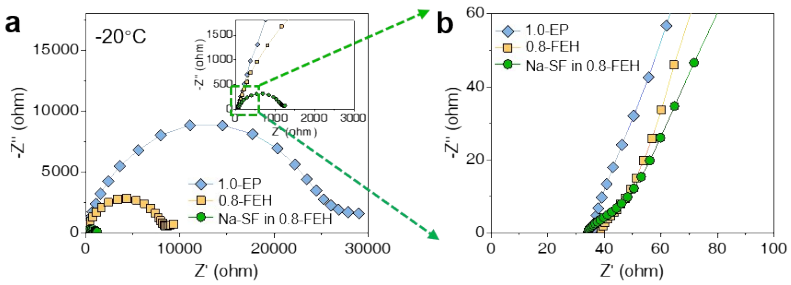


**Figure S12.** (a) The Nyquist plots of the Na/Na symmetric cells at -20°C after 3 formation cycles, with the (b) zoomed-in image on the right side, which displays the intercept on real-axis at high frequency representing the $R_e$ value from the equivalent circuit model shown in Figure S11.

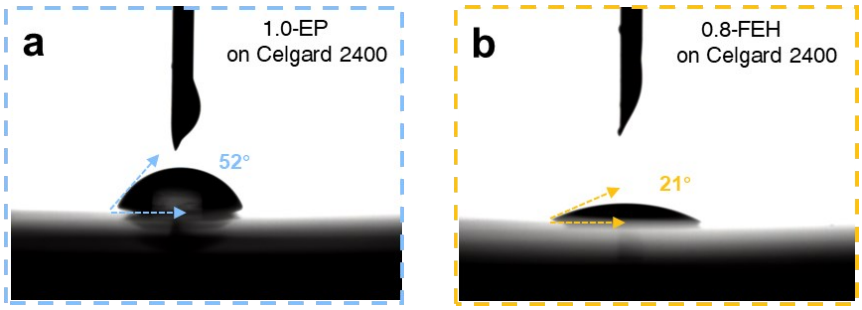


**Figure S13.** Wettability tests of the (a) 1.0-EP and (b) 0.8-FEH electrolyte on a Celgard 2400 polypropylene separator with labelled contact angles.

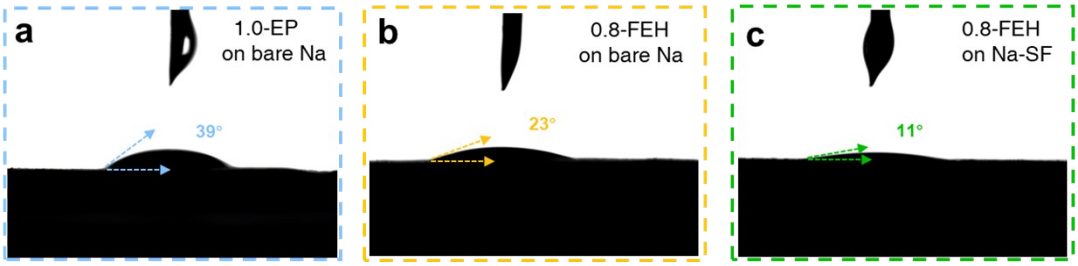


**Figure S14.** Wettability tests of the (a) 1.0-EP and (b) 0.8-FEH electrolyte on bare Na and the (c) 0.8-FEH electrolyte on Na-SF electrode with labelled contact angles. The reduced electrolyte contact angle on the electrode is beneficial not only to reduce the interfacial impedance, but also to mitigate $Na^+$ concentration gradient at the electrode surface.[15, 16]

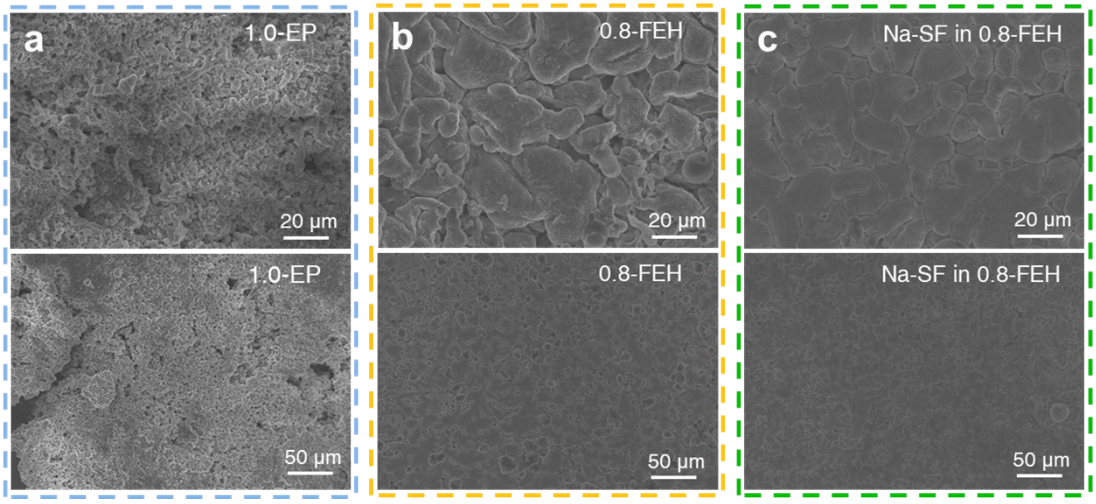


**Figure S15.** Top-view SEM images of the deposition morphology with bare Na in (a) 1.0-EP and (b) 0.8-FEH electrolytes, and (c) Na-SF anode in the 0.8-FEH electrolyte with various magnificantions at 25℃.

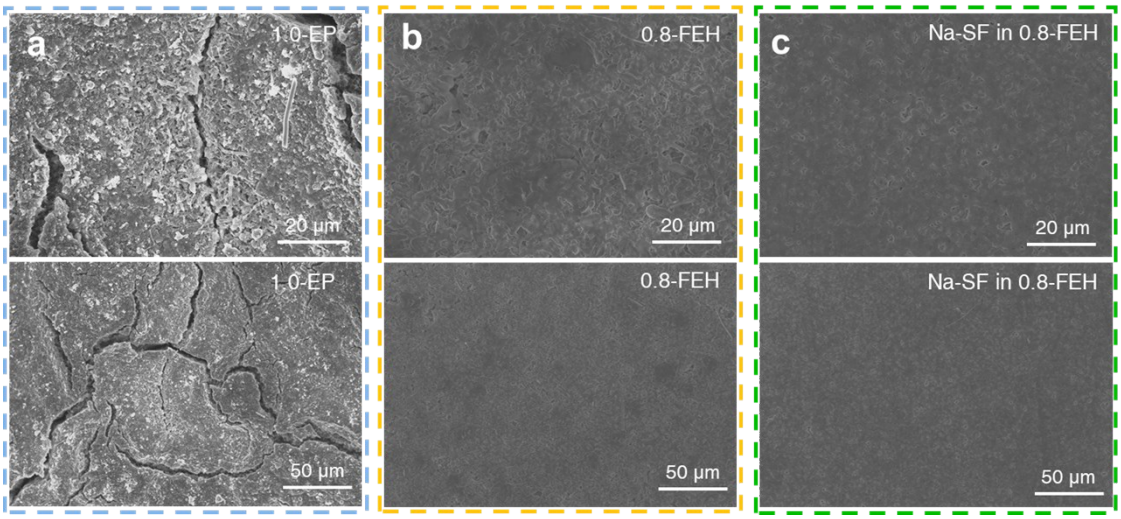


**Figure S16.** Top-view SEM images of the deposition morphology with bare Na in (a) 1.0-EP and (b) 0.8-FEH electrolyte, and (c) Na-SF anode in the 0.8-FEH electrolyte with various magnificantions at -20℃.

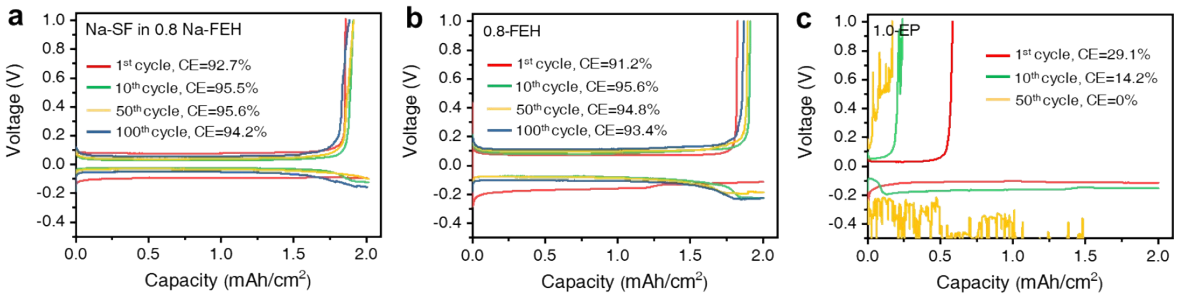


**Figure S17.** The corresponding Na plating/stripping voltage profiles on Cu electrode with (a) Na-SF in 0.8-FEH electrolyte, and bare Na in the (b) 1.0-EP, (c) 0.8-FEH electrolytes at 1.0 mA/cm$^2$ with a capacity of 2.0 mAh/cm$^2$.

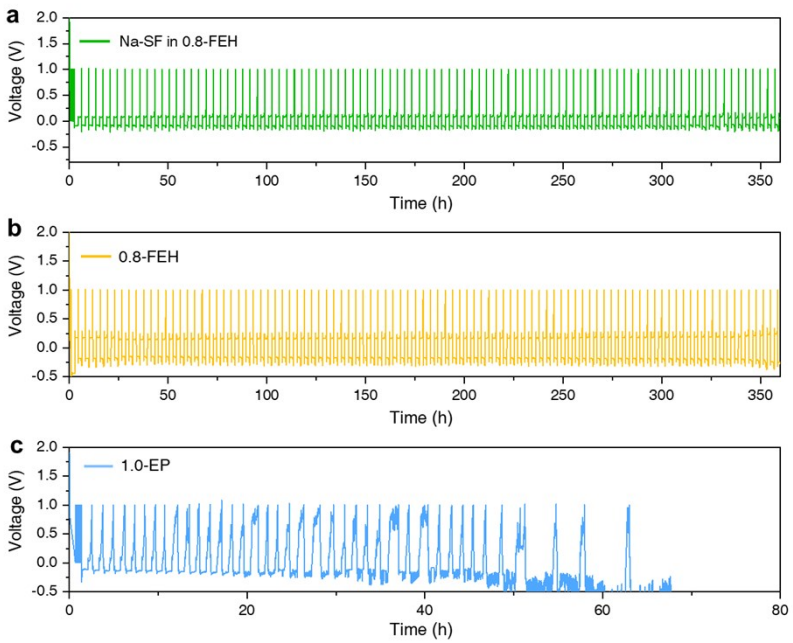


**Figure S18.** Voltage-time profiles of Na plating/stripping with (a) Na-SF electrode in the 0.8-FEH electrolyte, and bare Na electrode in the (b) 0.8-FEH and the (c) 1.0-EP electrolytes.

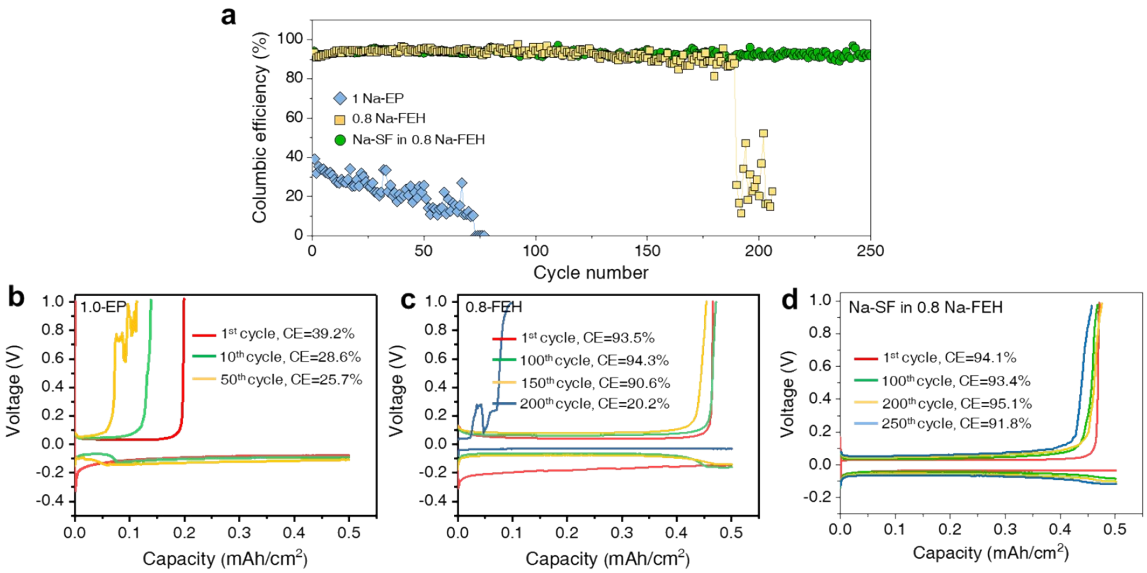


**Figure S19.** (a) CE of Na plating/stripping at 0.5 mA/cm$^2$, 0.5 mAh/cm$^2$ with the corresponding systems. The corresponding Na plating/stripping voltage profiles on Cu electrode with bare Na in (b) 1.0-EP, (c) 0.8-FEH and (d) Na-SF in 0.8-FEH.

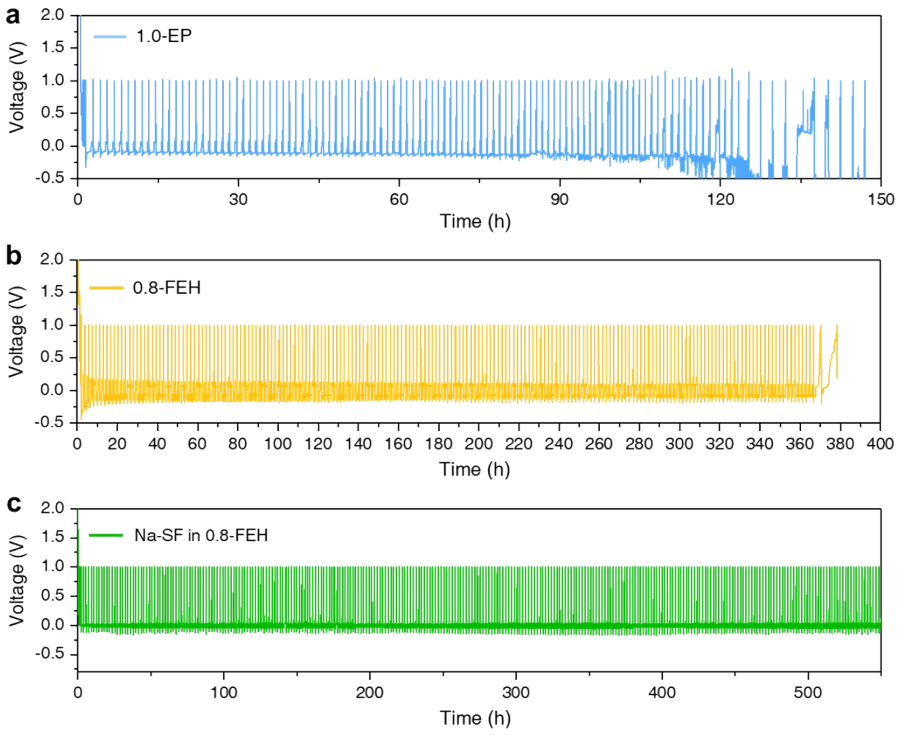


**Figure S20.** Voltage-time profiles of Na plating/stripping with bare Na electrode in (a) 1.0-EP and (b) 0.8-FEH electrolytes, and (c) Na-SF electrode in the 0.8-FEH electrolyte at 0.5 mA/cm$^2$, 0.5 mAh/cm$^2$.

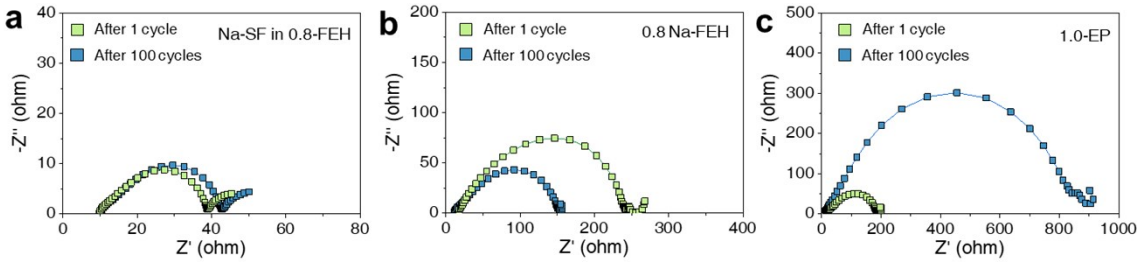


**Figure S21.** Nyquist plots of the symmetric cells after 1st and 100th cycles with bare Na electrode in the (a) 1.0 EP (b) and 0.8-FEH electrolyte, and the (c) Na-SF electrode in the 0.8-FEH electrolyte. The restricted increment in the interfacial resistance observed with Na-SF in 0.8-FEH electrolyte ascertains a stabilized Na/electrolyte interface, whereas the spiking resistance (~900 Ω) seen using bare Na in 1.0-EP electrolyte indicates the fast deteriorated interface as a result of the sustained parasitic reactions, which are commonly observed using the conventional carbonate-based electrolyte.[17, 18]

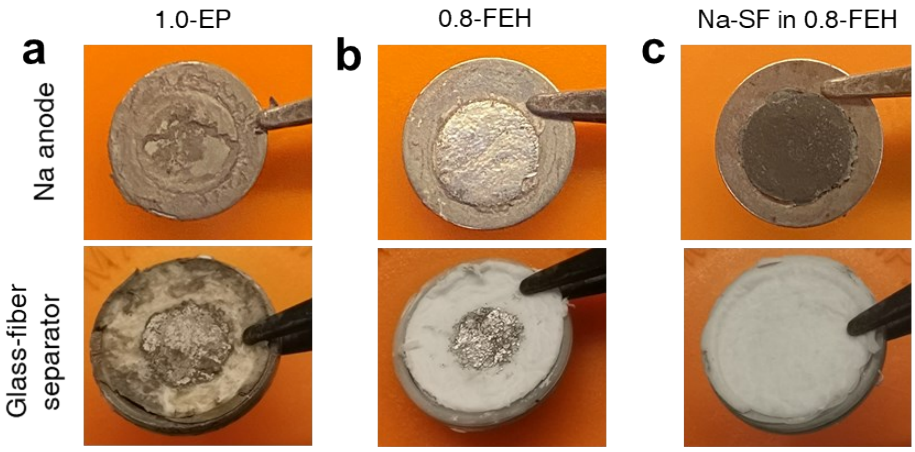


**Figure S22.** Optical images of the bare Na metal anode and the glass-fiber separators after 100 cycles in the (a) 1.0-EP and the (b) 0.8-FEH electrolyte. (c) The Na-SF electrode and the corresponding glass-fiber separator after 100 cycles in the 0.8-FEH electrolyte. The electrodes and separators are all retrived from the cycled symmetric cells. In contrast to the pulverized Na metal (brown grey color) after cycling in the 1.0-EP electrolyte, the counterpart Na retrieved from the 0.8-FEH electrolyte still retained its silver metallic cluster. The amount of dead Na inserted in the separator was also massively decreased, indicating of the less parasitic reactions and thus the Na-compatibility of the 0.8-FEH electrolyte. By using Na-SF electrode in 0.8-FEH, its black surface layer, which is the $Na_{15}Sn_4$/NaF biphasic ASEI, has maintained compact and coherent. More surprising is the eliminated dead Na layer on the separator by employing Na-SF electrode, which is critical not only for safety-enhancement but also for guaranteeing high plating/stripping CE over the long-term.[19]

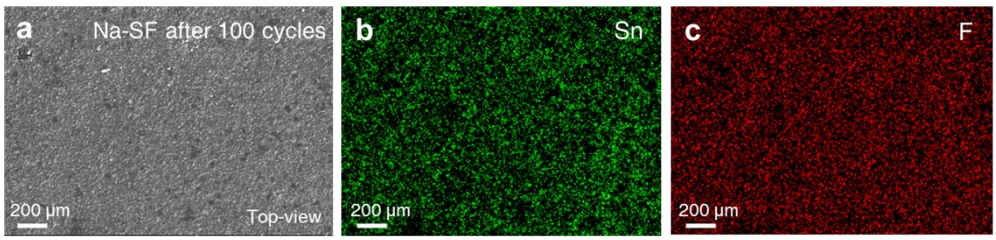


**Figure S23.** (a) Top-view SEM image with the corresponding EDX mapping of the (b) Sn and (b) F signal on the retrieved Na-SF electrode after 100 cycles using the 0.8-FEH electrolyte. The EDX analysis verifies strong signals of Sn and F element covering on the cycled Na-SF electrode, indicative of the validity of the as-formed $Na_{15}Sn_4$/NaF biphasic ASEI to stay unperturbed upon cycling.

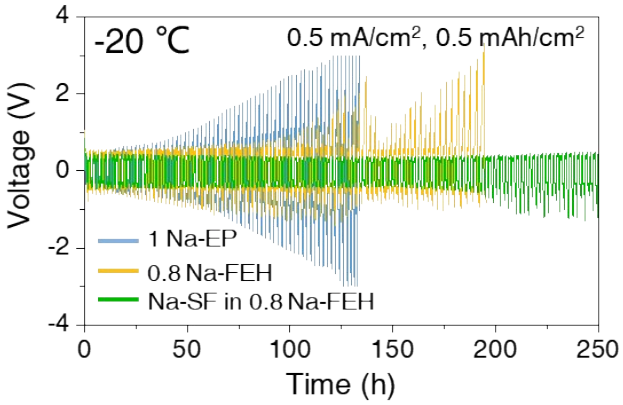


**Figure S24.** Galvanostatic plating/stripping of the symmetric cells at 0.5 mA/cm$^2$, 0.5 mAh/cm$^2$ at -20℃.

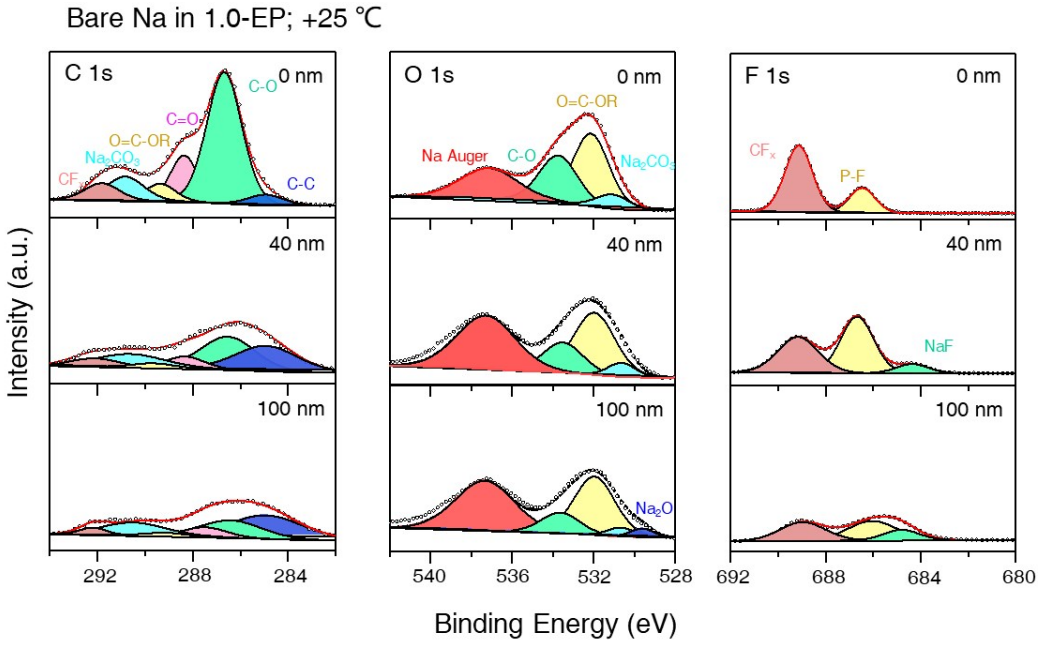


**Figure S25.** In-depth C 1s, O 1s and F 1s XPS spectra of the bare Na anode after 20 cycles in the 1.0-EP electrolyte at an operation temperature of 25℃.

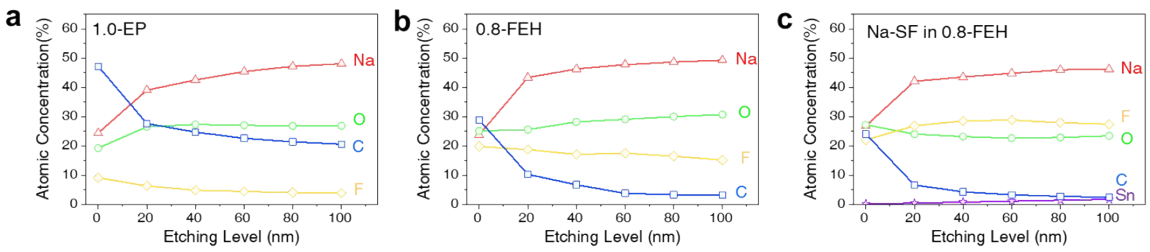


**Figure S26.** Atomic ratios of Na, O, C, F and Sn signals in the SEI of bare Na in the (a) 1.0-EP electrolyte and the (b) 0.8-FEH electrolyte, and (c) Na-SF anode in the 0.8-FEH electrolyte with proceeding sputtering depth after operating for 20 cycles at room-temperature (25℃).

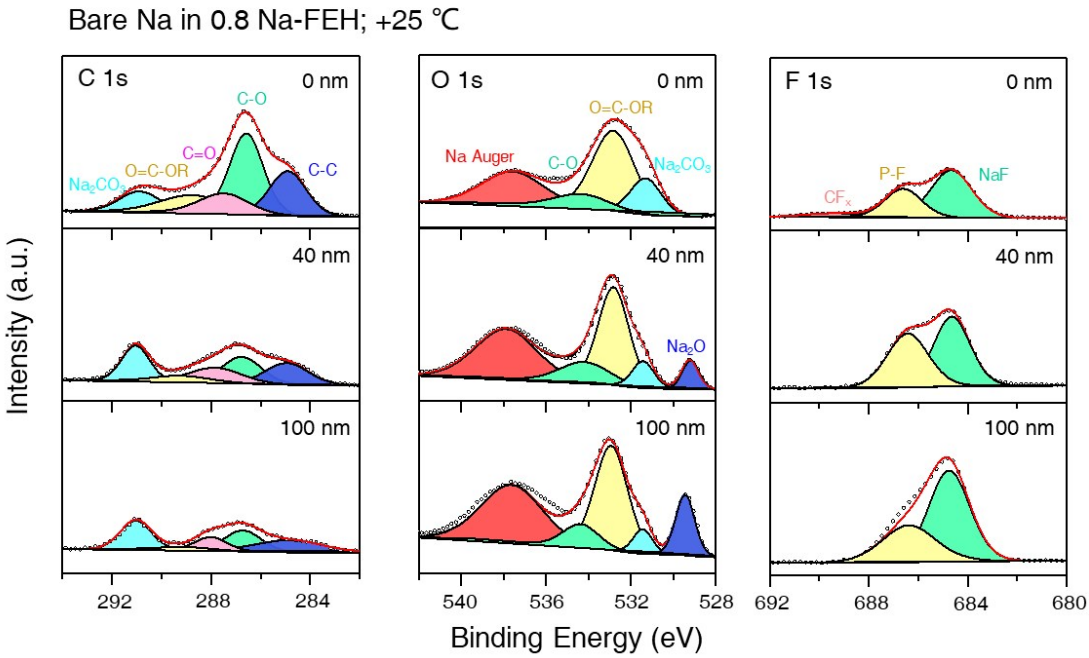


**Figure S27.** In-depth C 1s, O 1s and F 1s XPS spectra of the bare Na anode after 20 cycles in the 0.8-FEH electrolyte at an operation temperature of 25℃.

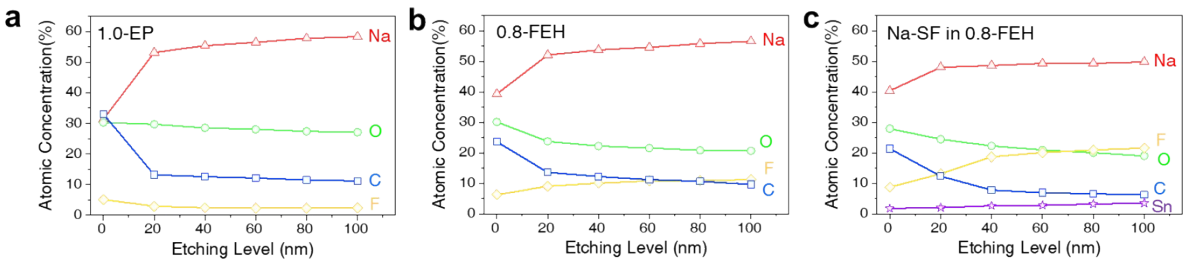


**Figure S28.** Atomic ratios of Na, O, C, F and Sn signals in the SEI of bare Na in the (a) 1.0-EP electrolyte and the (b) 0.8-FEH electrolyte, and (c) Na-SF anode in the 0.8-FEH electrolyte with proceeding sputtering depth after operating for 20 cycles at -20℃.

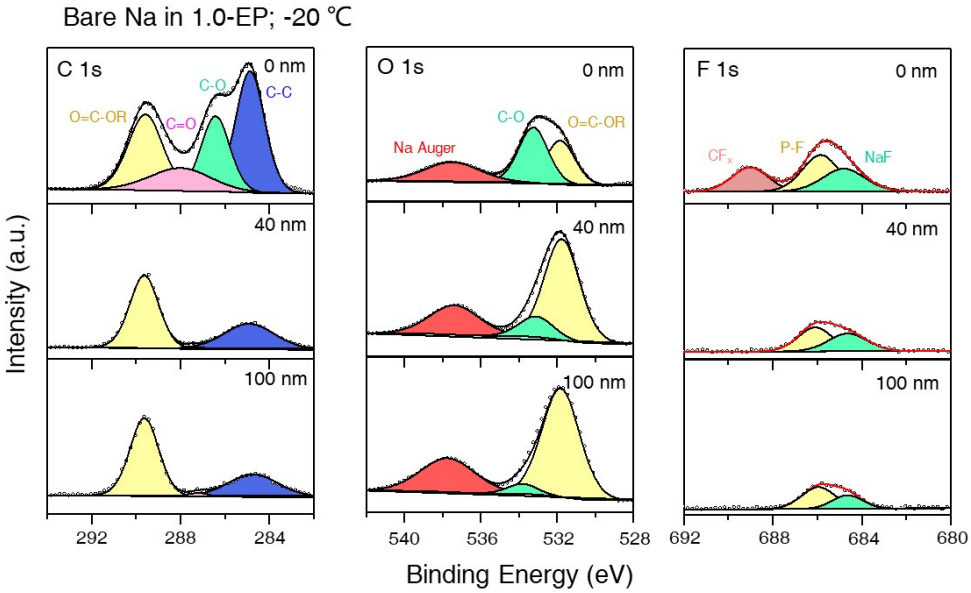


**Figure S29.** In-depth C 1s, O 1s and F 1s XPS spectra of the bare Na anode after 20 cycles in the 1.0-EP electrolyte at an operation temperature of -20℃.

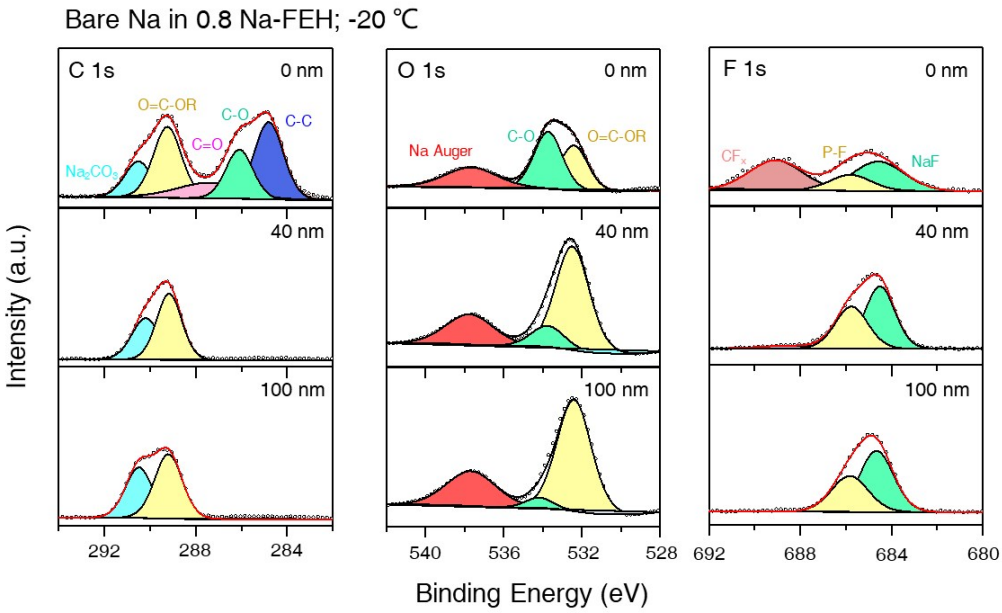


**Figure S30.** In-depth C 1s, O 1s, F 1s and Sn 3d XPS spectra of the bare Na anode after 20 cycles in the 0.8-FEH electrolyte at an operation temperature of -20℃.

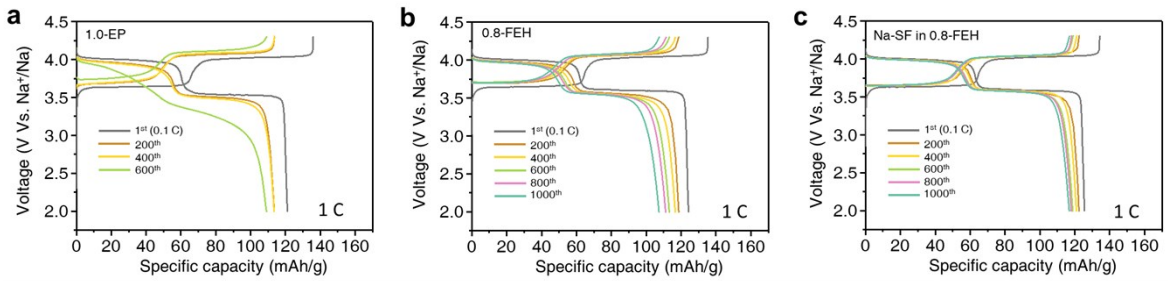


**Figure S31.** The corresponding voltage profiles of the Na/NVPOF full cells at various cycles under 1 C with bare Na in the (a) 1.0-EP and the (b) 0.8-FEH electrolyte, and (c) Na-SF anode in the 0.8-FEH electrolyte.

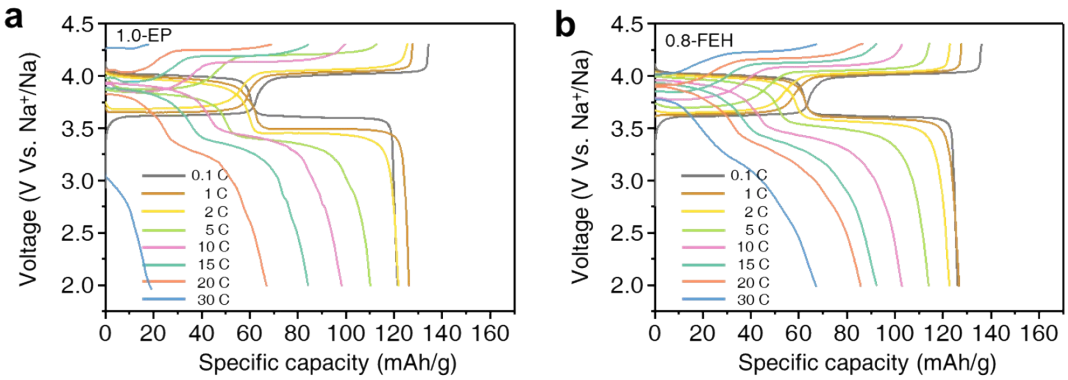


**Figure S32.** The corresponding voltage profiles of the Na/NVPOF full cells at rates from 1 C to 30 C in the (a) 1.0-EP and the (b) 0.8-FEH electrolyte. Three formation cycles were conducted at 0.1 C for film formation.

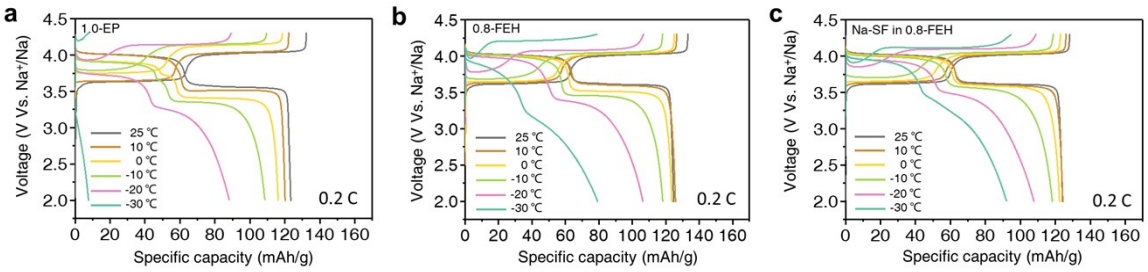


**Figure S33.** The corresponding voltage profiles of the Na/NVPOF full cells at temperatures from 25℃ to -30℃ under 0.2 C with bare Na in the (a) 1.0-EP and the (b) 0.8-FEH electrolyte, and (c) Na-SF anode in the 0.8-FEH electrolyte.

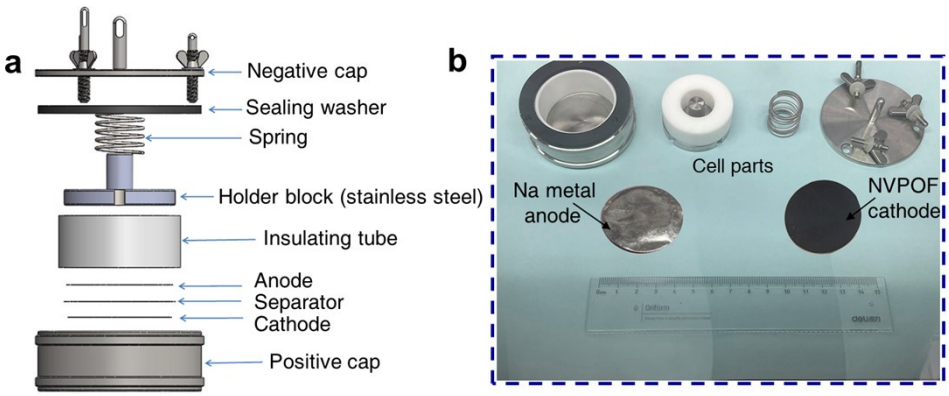


**Figure S34.** (a) Schematic illustration of the home-made cell model, with the (b) optical images of the cell parts. The cell model consists of negative cap, positive cap, spring and the holder block. An insulating tube is inserted here to prevent the contact between the cathode and the anode. Optical images of the cell parts are shown on the right side (Figure R4b), and the Na metal anode and the NVPOF cathode are both in the size of 42 mm in diameter.

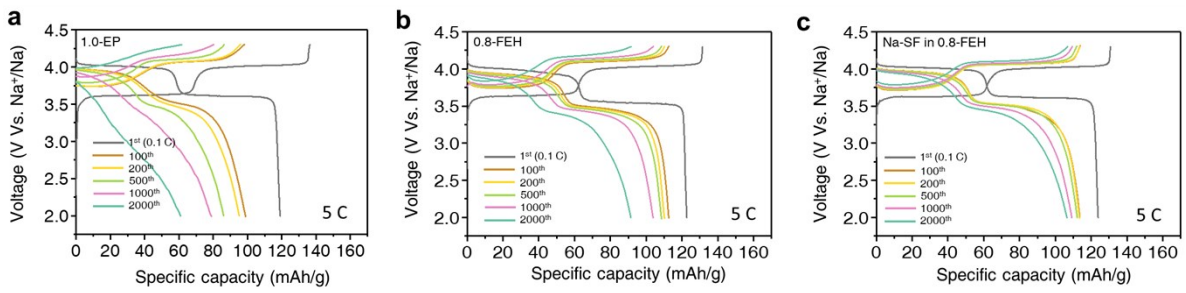


**Figure S35.** The corresponding voltage profiles of the Na/NVPOF full cells at various cycles under 5 C with bare Na in the (a) 1.0-EP and the (b) 0.8-FEH electrolyte, and (c) Na-SF anode in the 0.8-FEH electrolyte.

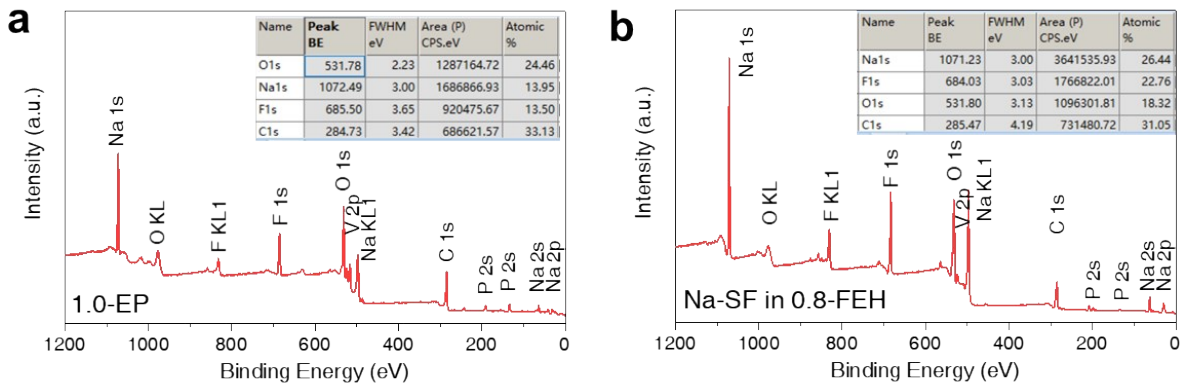


**Figure S36.** Full survey XPS spectra of the cycled NVPOF cathode in the (a) 1.0-EP and the (b) 0.8-FEH electrolytes.

**Table S1.** Physical characteristics of the corresponding electrolyte solvent.[20, 21]

| Solvent | Dielectric constant (ε) | Donor Number (DN) | Viscosity at RT (mPa s) | Melting point |
|---|---|---|---|---|
| **EC** | 89.8 | 16.4 | 1.95 (at 40°C) | 36°C |
| **PC** | 64.9 | 15.1 | 2.5 | -48°C |
| **FEC** | 78.4 | 9.1 | 3.3 | 20°C |
| **EMC** | 2.4 | 16 | 0.65 | -55°C |
| **HFE** | - | - | - | -94°C |

**Table S2.** The calculated coordination number of the corresponding solvent molecules or anions in the 1.0-EP and the 0.8-FEH electrolyte.

| Electrolyte | Coordination number | | | | | |
|---|---|---|---|---|---|---|
| | EC | PC | FEC | EMC | HFE | $PF_6^-$ |
| 1.0-EP | 2.756 | 2.345 | - | - | - | 0.1236 |
| 0.8-FEH | - | - | 1.752 | 1.822 | 0.1198 | 0.4182 |

**Supplementary References**


1. Z.-Y. Gu, J.-Z. Guo, Z.-H. Sun, X.-X. Zhao, W.-H. Li, X. Yang, H.-J. Liang, C.-D. Zhao and X.-L. Wu, *Sci. Bull.*, 2020, **65**, 702-710.
2. M. J. Abraham, T. Murtola, R. Schulz, S. Páll, J. C. Smith, B. Hess and E. Lindahl, *SoftwareX*, 2015, **1-2**, 19-25.
3. S. V. Sambasivarao and O. Acevedo, *J. Chem. Theory Comput.*, 2009, **5**, 1038-1050.
4. B. Doherty, X. Zhong, S. Gathiaka, B. Li and O. Acevedo, *J. Chem. Theory Comput.*, 2017, **13**, 6131-6145.
5. L. S. Dodda, I. Cabeza de Vaca, J. Tirado-Rives and W. L. Jorgensen, *Nucleic Acids Res.*, 2017, **45**, W331-W336.
6. L. Martínez, R. Andrade, E. Birgin and J. Martínez, *J. Comput. Chem*, 2009, **30**, 2157-2164.
7. G. Bussi, D. Donadio and M. Parrinello, *J. Chem. Phys.*, 2007, **126**, 014101.
8. H. J. Berendsen, J. v. Postma, W. F. van Gunsteren, A. DiNola and J. R. Haak, *J. Chem. Phys.*, 1984, **81**, 3684-3690.
9. T. Darden, D. York and L. Pedersen, *J. Chem. Phys.*, 1993, **98**, 10089-10092.
10. W. Humphrey, A. Dalke and K. Schulten, *J. Molec. Graphics*, 1996, **14**, 33-38.
11. C. Adamo and V. Barone, *J. Chem. Phys.*, 1999, **110**, 6158-6170.
12. F. Weigend and R. Ahlrichs, *Phys. Chem. Chem. Phys.*, 2005, **7**, 3297-3305.
13. K. Xu, S. Zhang, J. L. Allen and T. R. Jow, *J. Electrochem. Soc.*, 2002, **149**, A1079.
14. G. Nagasubramanian and C. J. Orendorff, *J. Power Sources*, 2011, **196**, 8604-8609.
15. X. B. Cheng, T. Z. Hou, R. Zhang, H. J. Peng, C. Z. Zhao, J. Q. Huang and Q. Zhang, *Adv. Mater.*, 2016, **28**, 2888-2895.
16. X. Zheng, W. Yang, Z. Wang, L. Huang, S. Geng, J. Wen, W. Luo and Y. Huang, *Nano Energy*, 2020, **69**, 104387.
17. S.-S. Chi, X.-G. Qi, Y.-S. Hu and L.-Z. Fan, *Adv. Energy Mater.*, 2018, **8**, 1702764.
18. Q. Pang, X. Liang, I. R. Kochetkov, P. Hartmann and L. F. Nazar, *Angew. Chem. Int. Ed.*, 2018, **130**, 9943-9946.
19. X. Zheng, Z. Gu, X. Liu, Z. Wang, J. Wen, X. Wu, W. Luo and Y. Huang, *Energy Environ. Sci.*, 2020, **13**, 1788-1798.
20. W. M. Haynes, *CRC handbook of chemistry and physics*, CRC press, 2014.
21. K. Xu, *Chem. Rev.*, 2004, **104**, 4303-4418.